ARTICLE

Journal of Materials Chemistry
www.rsc.org/materials

On-line analysis of CdSe nanoparticle formation in a continuous flow chip-based microreactor

S. Krishnadasan, J. Tovilla, R. Vilar, A. J. deMello and J. C. deMello*

Department of Chemistry, Imperial College London, South Kensington, London, UK SW7 2AY. E-mail: j.demello@ic.ac.uk

Received 2nd February 2004, Accepted 20th May 2004
First published as an Advance Article on the web 1st July 2004

The online analysis of cadmium selenide nanoparticle formation in continuous-flow microfluidic reactors is described. The as-produced particles exhibit sharp excitonic absorption and emission peaks (~30–40 nm) with relatively high quantum efficiencies (~10%). The mean size and dispersity of the particles, determined using on-line fluorescence detection, may be controlled by varying the reaction temperature and/or the flow rate. The microfluidic approach provides considerable control over nucleation/growth processes and is a promising strategy for the direct production of near-monodisperse nanoparticles without recourse to further size selection.

Introduction

Nanocrystalline colloidal semiconductors are of considerable scientific and commercial interest owing to their tuneable optical and electronic properties and their applications in electronic devices and biosensors.[1] The physical characteristics of nanocrystallites are determined primarily by spatial confinement effects with properties such as the optical band gap often differing considerably from the bulk semiconductor. As these properties are ultimately determined by the physical dimensions of the crystallites, there is considerable interest in processing routes that yield nanoparticles of well defined size and shape.[2] In practice, for many applications, deviations about the mean particle radius must be lower than one percent.[3] This is beyond the tolerance of most standard syntheses (which rarely yield size distributions better than ±5%†), and in general it is necessary to employ some form of post-treatment to extract the desired particle size; typical treatments include electrophoresis,[8] chromatography,[9] sedimentation precipitation,[10] and photo-corrosion.[11] In this manner, it is possible to obtain nanoparticles with extremely narrow size distributions (better than ±5%). However, since the starting point is a polydisperse sample from which the desired particle size must be subsequently isolated, yields are generally low. It would be preferable to use *direct* techniques, requiring no post-treatment, to prepare the crystals.

In a previous paper[12] we reported that the synthesis of cadmium-sulfide nanoparticles in a continuous flow microfluidic reactor led to the formation of particles with improved monodispersity. We reported that the general strategy was applicable to a broad range of nanoparticles syntheses, and that it offered a promising strategy for synthesising near-monodisperse nanoparticles directly and without recourse to subsequent recrystallisations. Chan *et al.*[13] have subsequently reported the synthesis of CdSe nanoparticles in a microfluidic reactor by reacting $Cd(CH_3)_2$ with selenium dissolved in boiling trioctylphosphine oxide (TOPO). In some respects CdSe is a preferable material to CdS for research purposes owing to the extensive characterisation of its optoelectronic properties.[5] Chan *et al.* reported nanoparticles with full width half maxima (FWHM) of ~40 nm, broadly comparable to those derived from conventional bulk syntheses. They further reported that the peak wavelength could be varied from 528 nm to 545 nm in a straightforward manner by changing the reaction temperature from 180 to 210 °C, allowing fine control over the optical properties of the resultant particles. However $Cd(CH_3)_2$ – like many other organometallic cadmium sources – is pyrophoric and, following the work of Peng and coworkers,[14] most researchers have moved towards other precursors such as $Cd(AcO)_2$ and $CdCO_3$ which are easier to manipulate, commercially available, and non-explosive. In this paper, we report the synthesis of CdSe nanoparticles in a microfluidic chip based on the direct reaction of Se and $Cd(AcO)_2$ dissolved in a mixture of TOPO and TOP (trioctylphosphine). A microreactor-based route to CdSe nanoparticles based on the $Cd(AcO)_2$ precursor has previously been reported by Nakamura *et al.*,[15] who used a capillary immersed in an oil-bath to perform the reaction. A similar approach was used by Yen *et al.*[16] who synthesised nanoparticles from cadmium oleate and TOP/Se using a heated glass capillary. In both cases, the particles were analysed off line using absorption and/or fluorescence spectroscopy. In principle, the use of microfluidic chip-based reactors to perform the reactions allows greater complexity in system design and improved scalability[13] but, more importantly for the current purposes, it also permits the use of online fluorescence detection to monitor particle formation during the reaction. In this manuscript we describe a simple on-line synthesis and analysis system that permits preparation and monitoring of particles in real-time. Systems of this nature may in future allow for intelligent feedback-driven processing, in which reaction variables such as temperature and flow rate are continuously updated to correct for any changes in environmental conditions that may occur as the reaction proceeds; an important example in the current context might be the ability to modify flow dynamics in response to particle deposition on the channel walls, thereby achieving improved long term operating stability.

Experimental details

A glass microfluidic reactor was fabricated in-house and used for the synthesis of CdSe nanoparticles. Channels were created using standard photolithographic procedures followed by wet chemical etching and bonding techniques. Briefly, a positive photoresist (S 1818, Shipley Corporation) was spin-coated

† For some previous reports where direct methods are employed to yield QDs with size distributions around ±5% see refs. 4–7 and references therein.

DOI: 10.1039/b401559b

onto the surface of a glass substrate (SLW, Hoya Corporation), and the channel design transferred to the substrate using a direct write laser lithography system (DWL2.0, Heidelberg Instruments). After soft-baking (95 °C for 1 min) and exposure, the exposed regions of the photoresist were removed using a developer (Microposit 351, Shipley) and the remaining photoresist hard-baked (95 °C for 5 min). Channels were then etched into the substrate using a buffered oxide etching solution (HF/NH_4F) at ambient temperature. Once complete, the etched substrate was sonicated sequentially in acetone, H_2SO_4/H_2O_2 and ultra pure water at ambient temperature, and dried with N_2 gas. Finally, a cover plate was thermally bonded to the substrate by heating the assembly at 550 °C for 1 h, 600 °C for 6 h and 555 °C for 1 h. The complete device was then allowed to cool for 8 hours. Holes drilled in the top plate allowed access to the fluidic network below. The reaction microchannel was 170 μm wide and 80 μm deep with a surface roughness (absolute-roughness/channel-diameter) of ±2.5%. The channel length was 40 cm. The microchannel architecture is indicated in the inset to Fig. 1.

Selenium powder (9.5 mg) was dissolved in trioctylphosphine (TOP, 2 ml) under a dry nitrogen atmosphere with vigorous stirring. $Cd(AcO)_2$ (6.5 mg) and technical grade (90%) trioctylphosphine oxide (TOPO) (300 mg) were added to the solution. A syringe pump (PHD 2000, Harvard Instruments) was used to deliver the precursor solution into the microfluidic channel at a variety of flow rates (0.25–10 μL min^{-1}). Nucleation and nanoparticle growth were initiated by placing the chip on a temperature-stabilised hotplate with high spatial temperature uniformity (Thickfilm Heater, Watlow), ensuring that variations in temperature across the reaction zone were less than 1 K.

The reaction products were monitored at ambient temperature in an observation zone down-stream of the reaction zone (and physically offset from the hot plate) in order to reduce thermal fluorescence quenching effects that often occur at high temperatures.‡. The 700 × 350 μm ($W \times H$) dimensions of the observation channel were chosen to be somewhat larger than those of the reaction channel in order to improve detection efficiencies. The particles were excited using a 404 nm solid-state laser excitation source incident from one-side of the chip substrate, and emission was detected using a fibre-optic CCD spectrometer (S2000, Ocean Optics) positioned directly above the channel and normal to the chip substrate.

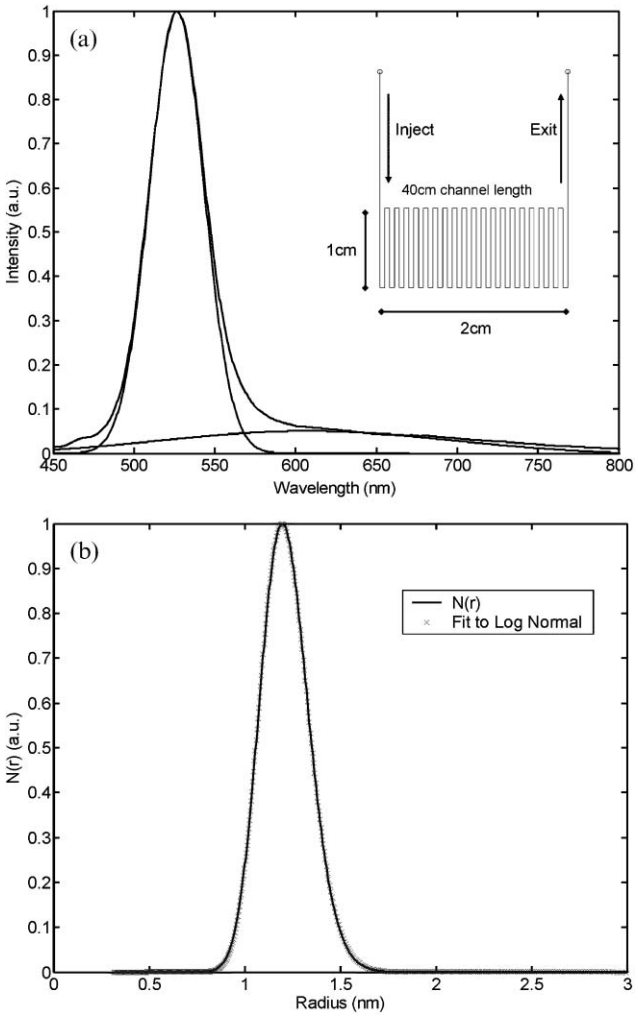

Fig. 1 (a) The emission spectrum for nanoparticles produced at a reaction temperature of 270 °C and a flow rate of 8 μL min^{-1} (other reaction conditions as stated in main text). The spectrum was measured online using a 404 nm laser diode excitation source and a CCD-spectrometer. The observed spectrum comprises a sharp Gaussian band-edge emission peak centred at 528 nm and a broad weaker peak centred at 605 nm due to recombination at surface defects. (b) The extracted size distribution of the particles shown in (a) as determined from the band-edge emission spectrum using Eq. (3). The size distribution is described well by a log-normal distribution.

Data analysis

The size distributions of the particles produced in the microreactors were determined from the profile of the band-edge emission using the approach of Garuthara and Levine.[17] The emission spectrum $I(\lambda)$ may be approximated as a convolution of the band edge emission spectrum $I(\lambda,r)$ for a single particle of radius r with the size distribution $N(r)$ of the population: $I \propto I(\lambda,r) \otimes N(r)$. In practice, $I(\lambda,r)$ is extremely narrow and may be approximated as a delta function $I(\lambda,r) = \delta\{\lambda - \bar{\lambda}(r)\}$ where $\bar{\lambda}(r)$ is the centre of the emission peak; using this approximation allows a direct mathematical inversion of the convolution, yielding a size distribution of the form:

$$N(r) \propto I(\lambda(r)) \cdot \frac{d\bar{\lambda}(r)}{dr} \tag{1}$$

We deviate slightly from the approach of Garuthara and Levine at this point. They determined $d\bar{\lambda}(r)/dr$ from the standard Brus Equation, which provides a good description of band-edge emission in larger particles but is less applicable to smaller particles of the kind investigated here. Here we use a modified Brus Equation proposed by Masumoto,[18] that allows for penetration of the electron a small distance l outside of the crystal core:

$$\begin{aligned} \overline{E}(r) &= E_G\left\{1+\frac{l_q^2}{(r+l)^2}\right\} \rightarrow \bar{\lambda}(r) = \frac{\lambda_G}{\left\{1+\frac{l_q^2}{(r+l)^2}\right\}} \rightarrow \bar{\lambda}(r) \\ &= \lambda_G\left\{\frac{(r+l)^2}{(r+l)^2+l_q^2}\right\} \end{aligned} \tag{2}$$

where E_G is the bulk energy gap, λ_G is the same value expressed in units of wavelength, $l_q = \pi\hbar/\sqrt{2m^*E_G}$ and m^* is the effective mass of the exciton. In ref. 5 Murray *et al.* reported emission data for a series of size monodisperse CdSe particles. We were able to achieve an excellent fit to their experimental data using Eq. (2) and the optimised parameter values l_q = 16.5 Å and

‡ The degree of quenching is dependent on the nature of the particles and the chosen synthesis route. In circumstances where such effects are weak – *e.g.* with room temperature syntheses – particle formation can be monitored within the reaction zone itself. For a fixed flow rate, the location along the flow profile correlates directly with reaction time and hence by monitoring fluorescence at multiple locations along the channel one may probe the real-time dynamics of particle formation. An equivalent effect was achieved here by fixing the location of the monitoring zone and varying the flow rate.

$l = 15.4$ Å; with these values we obtained a standard deviation of just ± 0.02 Å. Using these parameter values, Eq. (2) may then be combined with Eq. (1) to obtain an estimate for the size distribution based on the measured emission spectrum $I(\lambda)$:

$$\frac{d\bar{\lambda}}{dr} = \frac{2\lambda_G l_q^2 (r+l)}{\left[(r+l)^2 + l_q^2\right]^2} \rightarrow N(r) \propto \frac{2\lambda_G l_q^2 (r+l)}{\left[(r+l)^2 + l_q^2\right]^2} \cdot I(\lambda(r)) \quad (3)$$

In passing, we note that the use of Eq. (3) to determine size distributions has advantages over some alternative procedures for extracting size distributions from emission spectra: (i) it is based on an equation due to Masumoto that provides an excellent empirical fit to experimental data even for small particles sizes; and (ii) it does not assume a Gaussian line shape for emission. In common with other emission-based approaches, the analysis relies on the implicit assumption that fluorescence quantum efficiencies are independent of particle size. This is a reasonable assumption for narrow size distributions (where variations in quantum efficiency are likely to be small over the sample range) but may not be true for highly disperse ensembles.

Results and discussion

Fig. 1a shows the emission spectrum of nanoparticles obtained at an illustrative reaction temperature of 270 °C and a flow rate of 8 μL min^{-1}. The spectrum comprises a strong excitonic emission peak at 528 nm with FWHM of 41 nm, and a broad weaker peak at 605 nm due to radiative recombination at surface defects. The defect emission may be removed by extended thermal annealing but our intention here was to probe the real time kinetics of particle growth directly online and, therefore, we did not include any annealing stage. The measured photoluminescence quantum yield (photons emitted/photons absorbed) was 9%, which is relatively high for uncapped particles and is commensurate with the dominance of band-edge emission over (inefficient) surface defect related emission. The narrow band-edge emission, small measured Stokes shift (15 nm) and weak deep trap emission, indicate that the particle surface is fairly smooth and regular with relatively widely dispersed surface defects. Fig. 1b shows the corresponding size distribution of the particles as determined from Eq. (3) using the optimised values of $l_q = 16.5$ Å and $l = 15.4$ Å. The particles have a mean radius $\bar{r} = 1.14$ nm with a FWHM of $\Delta r = 0.42$ nm, which compares favourably with those prepared using conventional bulk syntheses. It should be noted that these size distributions are those of the untreated particles exiting the microfluidic channel, and that subsequent size selection could if necessary be used to obtain narrower size distributions. However our ultimate aim in this work is to develop techniques for the controlled and direct on-chip production of near-monodisperse particles ($\Delta r/\bar{r} < 5\%$) that require no further size selection before use. In this paper, we therefore examine the various factors that influence the mean size and dispersity of the untreated particles as they exit the reactors.

The extracted size distribution fits well to a log-normal distribution (solid line in Fig. 1b), and it seems to be a mathematical property of Eq. 3 that, if the emission spectrum $I(\lambda(r))$ is Gaussian in shape, the underlying size distribution $N(r)$ is approximately log-normal. The Gaussian nature of the band-edge emission from nanoparticles has been widely reported in the literature (see for example ref. 19 and references therein) suggesting that nanoparticles are frequently produced with a log normal distribution regardless of synthesis route; a similar conclusion (based on a different analysis of emission spectra) was drawn by Dushkin in ref. 19, and was attributed to the similarity of growth kinetics in different colloidal systems. The log normal nature of the size distributions is supported for instance by high resolution TEM images of CdSe nanoparticles synthesised in a hot amphiphile matrix and capped with TOPO and TOP;[19] other supporting evidence is provided in refs. 20–22.

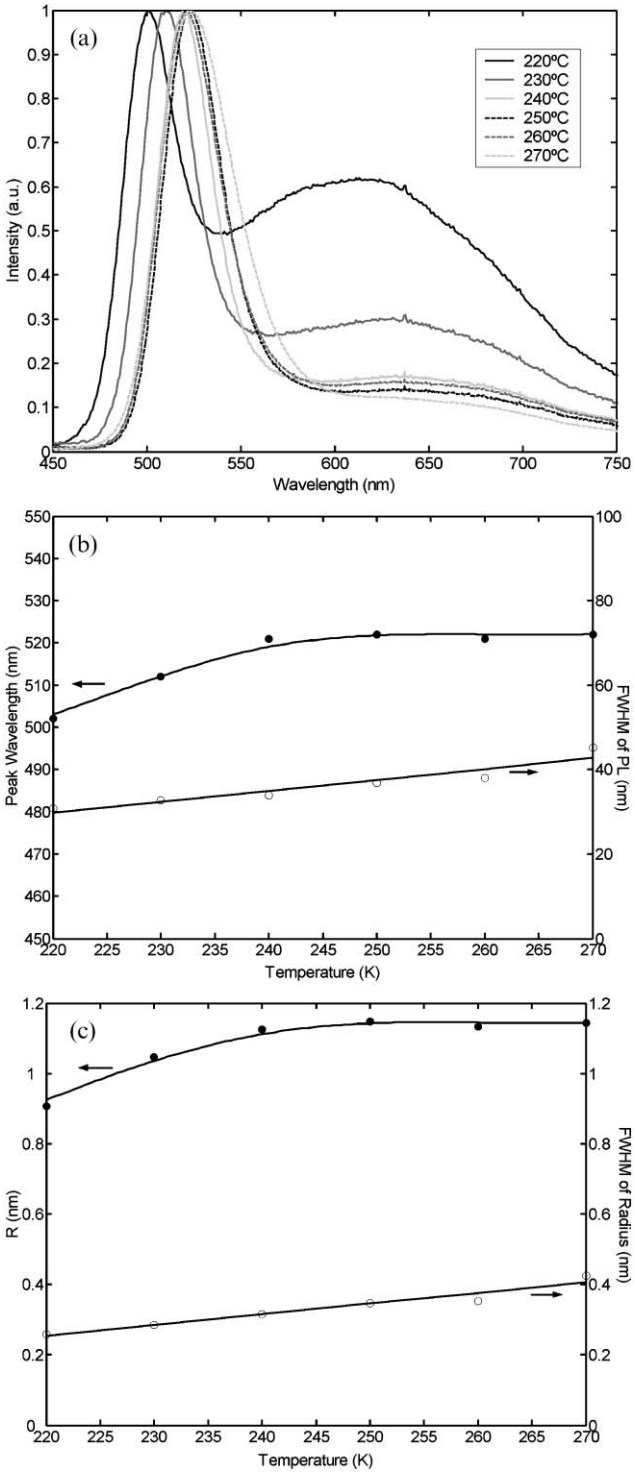

Fig. 2 (a) The emission spectra for particles produced at a flow rate of 8 μL min^{-1} and a variety of reaction temperatures in the range 220 to 270 °C. The spectra exhibit separate contributions from band-edge emission and from surface defects. (b) The temperature dependence of the peak position $\bar{\lambda}$ (solid dots) and the FWHM $\Delta\lambda$ (open dots) of the band-edge emission for the particles shown in (a). The emission peak shifts to longer wavelengths at higher temperatures, consistent with a higher reaction rate and increased growth, and shows a weak increase in FWHM with temperature. (c) The temperature dependence of the mean particle size $\bar{r}$ (solid dots) and the FWHM size dispersity Δr (open dots), as determined from the data in (a) using Eq. (3).

Fig. 2a shows the emission spectra for particles produced at a flow rate of 8 μL min^{-1} and at a variety of reaction

temperatures in the range 220 to 270 °C. At higher temperatures evolution of gas from the solvent mix was observed. This is probably due to impurities present in the technical grade TOPO used. This gas evolution limits the range of temperatures that can be accessed in the microfluidic reactor since bubbling is uncontrolled and introduces a degree of chaos into the flow dynamics, making it difficult to achieve stable operation. In common with the data in Fig. 1, all spectra exhibit separate contributions from band-edge emission and (low energy) deep trap emission. The band-edge emission peak shows a progressive shift to lower energies as the reaction temperature is increased, consistent with the formation of larger particles at higher temperatures. The temperature dependence of the emission peak $\bar{\lambda}$ is reproduced in Fig. 2b with the secondary ordinate indicating the FWHM $\Delta\lambda$ of the peak. In Fig. 2c we show the temperature dependence of the mean particle size $\bar{r}$ and the dispersity of the size distribution Δr (expressed as a FWHM) based on the analysis described above. The particle size may be varied from 0.90 nm to 1.14 nm by changing the temperature from 220 to 270 °C. The saturation of the emission peak at 1.14 nm suggests that the reaction mixture may be fully spent at higher temperatures. The dispersity shows a small increase at higher temperatures but appears to be relatively insensitive to reaction temperature. The intensity of deep trap emission from the particles however is strongly dependent on the reaction temperature, with smaller particles produced at lower reaction temperatures showing more deep trap emission. This is consistent with the increasing surface–volume ratio as the particle radius is reduced and the influence of surface defects becomes correspondingly higher; deviations from spherical symmetry may also be important. The dominant influence of surface defects on the optical properties of small (sub 2.5 nm) particles is well known, having for example been recently discussed by Landes *et al.*[23] and Dushkin.[19]

The data in Fig. 2 were obtained at a fixed flow rate of 8 μL min^{-1}. The flow rate determines the 'residence time' on chip and hence the total reaction time. At lower flow rates, the reaction mixture remains inside the heated channel for longer periods of time and, provided the reagents are not fully spent before exiting the chip, larger particles are expected. Fig. 3a shows the emission spectra for particles produced at a temperature of 230 °C and a variety of flow rates in the range 0.25 to 8 μL min^{-1} – the latter rate corresponding to the highest achievable stable flow rate for the 170 × 80 μm channel dimensions and the specific syringe pump used. The spectra exhibit separate contributions from band-edge emission and (low energy) deep trap emission. As expected, the band-edge emission peak shows a progressive shift to lower energies as the flow rate is reduced, consistent with the formation of larger particles at lower flow rates. The flow rate dependence of the emission peak $\bar{\lambda}$ is reproduced in Fig. 3b for clarity with the secondary ordinate again indicating the FWHM $\Delta\lambda$ of the peak. In Fig. 3c we show the flow rate dependence of the mean particle size $\bar{r}$ and the dispersity Δr based on the analysis described above. The particle size may be changed from 1.05 nm to 1.52 nm by varying the flow rate between 8 and 0.25 μL min^{-1}, with Δr showing a clear upwards trend with slower flow rates. The smallest particles, formed at the highest flow rates, again showed the strongest deep trap emission due to the dominant influence of surface defects.

The increased dispersity at lower flow rates is undesirable and has its origins in the non-uniform velocity profile of the reaction mixture through the channel.[24] The channel walls impart strong shear forces on the reaction mixture so, under an applied hydrodynamic pressure, a parabolic velocity profile is established over the cross section of the channel (see inset to Fig. 4), with the velocity equal to zero at the channel walls and reaching a maximum at the centre. The reaction mixture collected downstream at the channel outlet is therefore formed

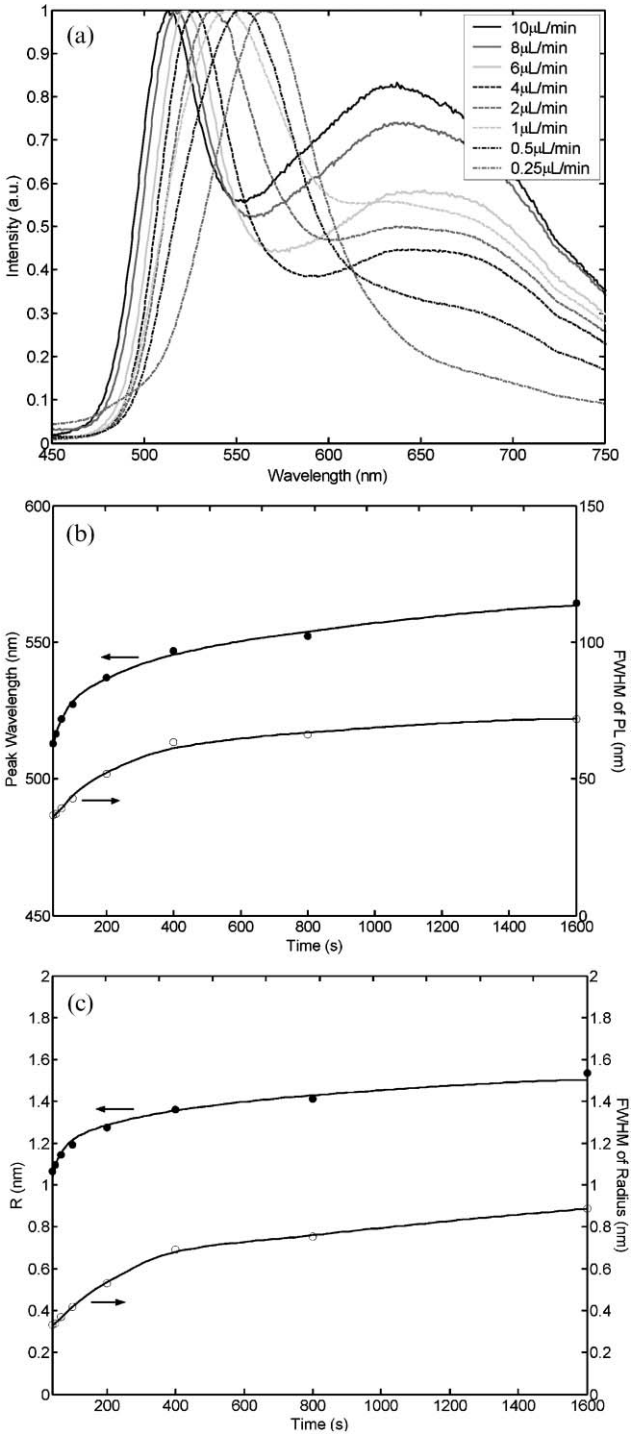

Fig. 3 (a) The emission spectra for particles produced at a temperature of 230 °C and a variety of flow rates in the range 0.25 to 8 μL min^{-1}. (b) The time dependence of the peak position $\bar{\lambda}$ (solid dots) and the FWHM $\Delta\lambda$ of the band-edge emission (open dots) for the particles shown in (a). The emission peak shifts to longer wavelengths at longer reaction times, consistent with the formation of larger particles. The FWHM shows a substantial increase with temperature. (c) The time dependence of the mean particle size $\bar{r}$ (solid dots) and the FWHM size dispersity Δr (open dots), as determined from the data in (a) using Eq. (3). The size dispersity increases substantially at longer mean residence times (slower flow rates), due to an increased broadening of the residence time distribution.

from an ensemble of volume elements that have spent different periods of time on chip. It is this distribution of residence times that primarily determines the final spread of particle sizes. In cylindrical channels, the parabolic velocity profile is described by $u(r) = 2\bar{u}(1 - r^2/R^2)$ where $\bar{u}$ is the mean velocity, and R is

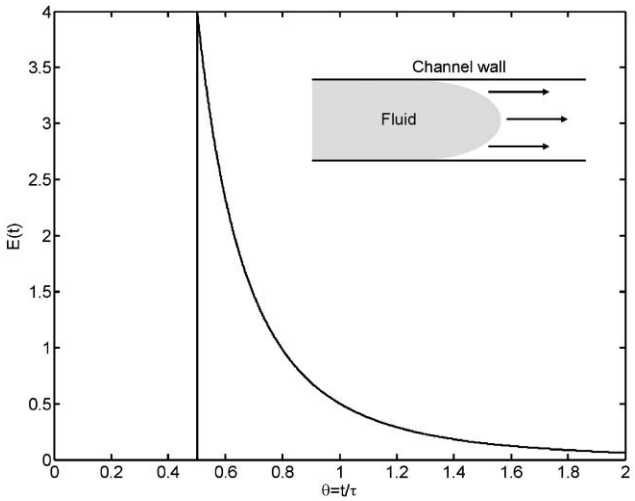

Fig. 4 The residence time distribution for volume elements of fluid passing through the chip, based on the assumption of a parabolic velocity profile. The channel walls impart strong shear forces on the reaction mixture so, under hydrodynamic pressure, a parabolic velocity profile is established across the cross section of the channel (see inset), with the velocity equal to zero at the channel walls and reaching a maximum at the centre. Fluid elements in the central flow spent only a relatively short amount of time on chip relative to those at periphery of the flow. Hence, a distribution of residence times results, whose width increases proportionally to the mean residence time. The dispersity of the particles increases with the width of the residence time distribution.

the channel radius.§ The mean residence time $\bar{\tau}$ is related to the channel length l by $\bar{\tau} = l/\bar{u}$. It is straightforward to show that the residence time distribution $E(t)$ is equal to $\bar{\tau}^2/2t^3$ in the range $\bar{\tau}/2 < t < \infty$, and is equal to zero elsewhere (see Fig. 4 and ref. 25). The lower limit $\bar{\tau}/2$ of the residence time distribution corresponds to the time required for the fastest moving volume elements at the centre of the channel (with velocity $2\bar{u}$) to travel a distance l. The width of the distribution $\Delta\tau$, defined as the time required for a fraction α of injected volume elements to emerge at the outlet channel, is determined by (4) and (5):

$$\alpha = \int_0^{\tau(\alpha)} E(t)\mathrm{d}t = \int_{\bar{\tau}/2}^{\tau(\alpha)} \left(\frac{\bar{\tau}^2}{2t^3}\right)\mathrm{d}t \rightarrow \tau(\alpha) = \frac{\bar{\tau}}{2\sqrt{1-\alpha}} \quad (4)$$

$$\Delta\tau(\alpha) = \tau(\alpha) - \bar{\tau}/2 = \frac{\bar{\tau}}{2}\left\{\frac{1}{\sqrt{1-\alpha}} - 1\right\} \quad (5)$$

The spread of residence times is therefore linearly proportional to the mean residence time, with for example $\Delta\tau(99\%)$ equal to 9 $\bar{\tau}/2$, and inversely proportional to the flow rate. In order to minimise the polydispersity of the particle population, it is necessary to minimise $\Delta\tau$, and hence high flow rates should be used. This is in agreement with the data from Fig. 3c. The influence of the velocity profile on the sample dispersity has also been noted by Yen *et al.*[16] In practice, the situation is rather more complex than we have described since the final size distribution depends on both the residence time effect and the growth dynamics of the particles. Fig. 3c indicates that the growth rate decreases with particle size – a situation which usually results in a narrowing of the size distribution over time (as smaller particles "catch-up" with larger ones) rather than the observed broadening. The reaction environment in the fluidic chip, however, is a complex one that behaves differently from a conventional bulk reactor: particles that form in the slow moving periphery flow spend much longer in the feedstock-rich upstream regions of the reactor than those formed in the faster central flow and therefore grow to a considerably larger size during their initial $\bar{\tau}/2$ of existence (and continue to grow thereafter) than the central particles do during their $\bar{\tau}/2$ residence on chip.¶ In consequence, the usual catch-up process does not occur and the size distribution continues to broaden with time. This is a fairly complex kinetic problem that will be analysed in more detail in a future manuscript.

§ In fact, the channels used in the current work were trapezoidal in shape but it will be sufficient for our current purposes to frame the discussion in terms of cylindrical channels.

Conclusion

The experimental findings provide insight into the optimum approach for fabricating near monodisperse nanoparticles in continuous flow microreactors. The key requirement is to minimise the width of the residence time distribution for volume elements passing through the reactor. In a simple reactor of the kind considered here, this may be achieved by operating the reactor at the maximum achievable stable flow rate to minimise the mean residence time and hence, by Eq. (5), $\Delta\tau$. The particle size may then be controlled by varying either the reaction temperature (Fig. 2) or alternatively by varying the composition of the reaction mixture. An alternative strategy is to reduce the transverse channel dimensions to allow Taylor dispersion conditions to prevail.[25] In these circumstances, transverse diffusion moves particles between different flow streams and, given a sufficient amount of time, each particle samples the entire distribution of flow velocities thereby reducing the overall spread in residence times. This effect is only appreciable when the diffusion range $\sqrt{2D\bar{\tau}}$ is comparable with the channel width d. Using the Stokes–Einstein relation $D = k_BT/6\pi\eta\gamma$, and assuming the average particle radius $r = 1$ nm and solvent viscosity $\eta = 15$ cP, we require $\bar{\tau} > d^2/2D \rightarrow \bar{\tau} > 1000$ s. Hence, for all but the slowest flow rates considered here, the effects of transverse diffusion on the residence time distribution may be ignored. However, if the channel dimensions were reduced by a factor 10–100, Taylor dispersion would dominate the colloidal flow characteristics leading to a reduction in fluid dispersion and, ultimately, a lower dispersity for the size distribution of particles. However, the advantages of this approach are lessened somewhat by an increased rate of colloid deposition on the channel surface. The rate of subsequent detachment is negligible even for smooth surfaces, leading to rapid clogging of the channel.[26] The successful direct synthesis of near monodisperse nanoparticles in microreactors will therefore depend on the implementation of novel channel architectures that ensure uniform (plug) flow without compromising reactor reliability. A second challenge relates to the on-chip formation of high quality small particles that have few surface defects and exhibit direct band-edge emission only. It is well established that the crystalline quality of cadmium chalcogenide particles may be improved by thermal annealing, which reduces the intensity of the long wavelength (trap-related) emission and enhances that of the band edge emission. It should be feasible to integrate such an annealing stage into the microfluidic chips (located downstream from the main reactor and following physical separation of the product from the reaction mixture) to improve the monochromacity and quantum efficiency of the emission. This is the subject of ongoing work.

In conclusion, we have investigated the use of microfluidic reactors for CdSe nanoparticle formation. The size of the particles may be controlled by varying the temperature and/or flow rate of the reaction mixture. It is preferable to use higher flow rates and temperatures to minimise the width of the

¶ The CdSe solutes are small and therefore distribute themselves evenly across the width of the channel. Therefore the large outer particles consume solutes from the entire width of the channel (rather than exclusively from their own radial volume element) and grow at the expense of the faster central particles.

residence time distribution and, hence, the polydispersity of the resultant particles. This approach yields high quality particles with high quantum efficiency and sharp emission characteristics, indicative of fairly monodisperse particles ($\Delta r/\bar{r} \sim 25\%$ at best). The smallest particles, produced at high flow rates and/or low temperatures, show broader emission and lower efficiencies due to the influence of surface defects.

Acknowledgements

The authors are grateful to EPSRC for financial support (S. K.) and CONACYT and ORS for a PhD studentship (J. T.).

References

1 A. P. Alivisatos, *Science*, 1996, **271**, 933.
2 M. A. Hines and P. Guyot-Sionnest, *J. Phys. Chem.*, 1996, **100**, 468.
3 B. A. Korgel and H. G. Monbouquette, *J. Phys. Chem.*, 1996, **100**, 346.
4 S. L. Cumberland, K. M. Hanif, A. Javier, G. A. Khitrov, G. F. Strouse, S. M. Woessner and C. S. Yun, *Chem. Mater.*, 2002, **14**, 1576.
5 C. B. Murray, D. J. Norris and M. G. Bawendi, *J. Am. Chem. Soc.*, 1993, **115**, 8706.
6 M. Green and P. O'Brien, *Chem. Commun.*, 1999, 2235.
7 X. Peng, *Chem. Eur. J.*, 2002, **8**, 334.
8 W. M. Hwang, C. Y. Lee, D. W. Boo and J. G. Choi, *Bull. Korean Chem. Soc.*, 2003, **24**, 684.
9 J. P. Novak, C. Nickerson, S. Franzen and D. L. Feldheim, *Anal. Chem.*, 2001, **73**, 5758.
10 J. T. G. Overbeek, *Adv. Colloid Interface Sci.*, 1982, **15**, 251.
11 S. T. Matsumoto, H. Mori and H. Yoneyama, *J. Phys. Chem.*, 1996, **100**, 13781.
12 J. B. Edel, R. Fortt, J. C. d. Mello and A. J. d. Mello, *Chem. Commun.*, 2002, 1136.
13 E. M. Chan, R. A. Mathias and A. P. Alivisatos, *Nano Lett.*, 2003, **3**, 199.
14 L. Qu, A. Peng and X. Peng, *Nano Lett.*, 2001, **1**, 333.
15 H. Nakamura, Y. Yamaguchi, M. Miyazaki, H. Maeda, M. Uehara and P. Mulvaney, *Chem. Commun.*, 2002, 2944.
16 B. K. H. Yen, N. E. Stott, K. F. Jensen and M. G. Bawendi, *Adv. Mater.*, 2003, **15**, 1858.
17 R. Garuthara and G. Levine, *J. Appl. Phys.*, 1996, **80**, 401.
18 Y. Masumoto, *J. Lumin.*, 1996, **70**, 386.
19 C. D. Dushkin, S. Saita, K. Yoshie and Y. Yamaguchi, *Adv. Colloid Interface Sci.*, 2000, **88**, 37.
20 E. M. Wong, J. E. Bonevich and P. C. Searson, *J. Phys. Chem. B*, 1998, **102**, 7770.
21 H. Weller, H. M. Schmidt, U. Koch, A. Fojtik, S. Baral and A. Henglein, *Chem. Phys. Lett.*, 1986, **124**, 557.
22 T. J. Goodwin, V. J. Leppert, S. H. Risbud, I. M. Kennedy and H. W. H. Lee, *Appl. Phys. Lett.*, 1997, **70**, 3122.
23 C. F. Landes, M. Braun and M. A. El-Sayed, *J. Phys. Chem. B*, 2001, **105**, 10554.
24 A. E. Kamholtz and P. Yager, *Biophys. J.*, 2001, **80**, 155.
25 K. Steffani and B. Platzer, *Chem. Eng. Process.*, 2002, **41**, 143.
26 S. C. James and C. V. Chrysikopoulos, *J. Colloid Interface Sci.*, 2003, **263**, 288.